ELSEVIER

Contents lists available at ScienceDirect

Carbon

journal homepage: www.elsevier.com/locate/carbon





Wearable room-temperature ethanol sensor based on Ti₃C₂T_x/Polypyrrole functionalized face mask for drunk driving monitoring

Guodong Wu^{a,1}, Haishun Du^{b,c,1}, Kiandokht Pakravan^a, Wonhyeong Kim^a, Yoo Lim Cha^a, Majid Beidaghi^a, Xinyu Zhang^b, Xuejun Pan^c, Dong-Joo Kim^{a,*}

- a Department of Materials Engineering, Auburn University, Auburn, AL, 36849, USA
- ^b Department of Chemical Engineering, Auburn University, Auburn, AL, 36849, USA
- ^c Department of Biological Systems Engineering, University of Wisconsin-Madison, 460 Henry Mall, Madison, WI, 53706, USA

ARTICLE INFO

Keywords: Ti₃C₂T_x Polypyrrole Disposable face mask Ethanol sensor Drunk driving monitoring

ABSTRACT

As one of the most encountered volatile organic compounds (VOCs), ethanol, especially with high blood concentrations, could cause adverse effects such as nausea, vomiting, skin allergies, low blood pressure, low blood sugar, and Parkinson's disease, seriously threatening human health and safety driving. In this study, we demonstrate a wearable ethanol sensor through drop-coating $Ti_3C_2T_x$ suspension followed by chemical polymerization of pyrrole on a disposable face mask substrate. The as-fabricated PP/ $Ti_3C_2T_x$ /PPy composite sensor exhibited a rapid response/recovery speed (49s/18s), a good sensing response of 76.3 % toward 400 ppm ethanol, an admirable theoretical limit of detection of 2.21 ppm, reliable flexibility, high selectivity, and excellent reproducibility. The outstanding sensing characteristics of the composite sensor are ascribed to the abundant functional groups (e.g., amino groups in PPy, terminal groups in $Ti_3C_2T_x$) and the formation of the Schottky junction between $Ti_3C_2T_x$ and PPy. Moreover, the composite sensor exhibits stable sensing performance around room temperatures (20–40 °C), and even at different bending states (0–150°). In addition, we developed a portable and wearable Bluetooth sensor module for human alcohol breath detection, suggesting the PP/ $Ti_3C_2T_x$ /PPy composite sensor can be used for human drunk driving monitoring and health assessment.

1. Introduction

Volatile organic compounds (VOCs) are significant hazardous air contaminants in industrial production and metropolitan life [1]. They evaporate into the environment at room temperature and atmospheric pressure, producing various harmful pollutants that can negatively affect the human nervous system, kidneys, and liver [2]. VOCs mainly include alcohols, acids, ketones, aldehydes, ethers, esters, etc., which can potentially lead to cancer and other major diseases, having long-term aggressive impacts on human health and air quality [3–5]. Besides, trace amounts of VOCs are present in the exhaled gases of the human body. They can serve as active biological markers for efficient early non-invasive disease analysis and diagnosis owing to their important physiological and metabolic-related information [6–8]. Among the VOCs, ethanol is the most widely used in biochemistry, pharmaceuticals, paints, and food and beverage industries [6,9,10]. Ethanol vapor is flammable that poses a vital risk of explosion and

combustion, with an explosion limit of 3.3–19.0 % [11,12]. According to the Occupational Safety and Health Administration (OSHA), exposure to ethanol vapor above 1000 ppm can cause headaches, drowsiness, difficulty in breathing, and adverse stimulation to the liver and eyes [13]. In addition, long-term exposure to ethanol environments as low as 25 ppm, may have negative effects on the human respiratory system, throat, and nervous systems, seriously threatening human health [14]. Furthermore, according to the accident survey conducted by the World Health Organization, approximately 50 %–60 % of traffic accidents are attributed to drunk driving, which has been identified as the primary cause of fatalities in such incidents [15]. Therefore, detecting the ethanol content in air condition and in the exhaled gases of vehicle drivers plays an important role in ensuring human health and avoiding drunk driving

Various methods such as tuning fork [18], photo-ionization detector (PID) [19], mass spectrometry (MS) [20], high-performance liquid chromatography (HPLC) [21], micro gas chromatography [22], and

E-mail address: dkim@auburn.edu (D.-J. Kim).

 $^{^{\}ast}$ Corresponding author.

 $^{^{1}\,}$ These authors contributed equally.

quartz crystal microbalances (QCM) [23] are widely used for precise detecting VOCs. However, these conventional techniques have some significant drawbacks, such as their large volume, time-consuming analysis, high energy consumption, and expensive and complicated equipment requirements [24-26]. Over the past two decades, researchers have shown considerable interest in developing gas sensors for monitoring inflammable, toxic, and harmful gases using p-type metal oxide semiconductors (MOSs) such as NiO [27], CuO [28], and Co₃O₄ [29], n-type MOSs like ZnO [30], TiO2 [31], and SnO2 [32], and perovskite-structured materials such as LaCoO₃ [33] and BaMnO₃ [34]. For instance, Zoolfakar et al. [35] developed an ethanol vapor gas sensor based on a highly crystalline and nanostructured p-type CuO, which was fabricated through radio frequency sputtering at a supply power of 200 W at 120°C. This sensor demonstrated remarkable sensing performance with a response value of 2.2 towards 12.5 ppm ethanol at an optimum operating temperature of 180°C. Qin et al. [36] synthesized a LaCoO₃/ZnO nano-flake composite through a sol-gel method. The LaCoO₃/ZnO sensor exhibited a response value of 55 towards 100 ppm ethanol at 320°C, which is six times higher than a pristine ZnO gas sensor. Nevertheless, these MOSs and perovskite-structured gas sensors have striking limitations, including high energy consumption, inflexible and fragile characteristics, and a requirement for high-temperature operation [37-39].

Currently, there is significant interest in developing portable, flexible, and room-temperature gas sensors for trace ethanol detection [40, 41]. Intrinsic conducting polymers (ICPs), such as polyaniline (PANI) [42,43], poly (styrene sulfonate) (PSS) [44], and polypyrrole (PPy) [45], have attracted substantial attention in gas sensors due to their easy synthesis, low operating temperature, good mechanical properties and electrical conductivity. However, the poor long-term stability and slow response time have limited their potential applications [42]. To address these issues, ICP-based composites, such as PANI/silver [46], PANI/TiO₂ [47], PPy/PVA [48], and PPy/ZnO [49], have been developed for ethanol sensing. For example, Yenorkar et al. [50] synthesized a PPy-MoO₃ composite film sensor for ethanol detection. The results showed that the composite sensor exhibited a sensitivity of 70%, which is 3.5 times higher than that of the pure PPy sensor.

Two-dimensional (2D) materials, such as black phosphorus (BP), graphene, graphene oxide (GO), hexagonal boron nitride (h-BN), and transition metal dichalcogenides (TMDs), have also been employed in flexible gas sensors due to their versatile surface chemistry, low electronic noise, large specific surface area, and outstanding electrical properties [2,51-53]. However, their relatively low sensitivity and interference from humidity limit their sensing applications. MXenes are relatively newly discovered 2D materials that have attracted wide attention in various fields, including sensors, biosensors, water purification, electromagnetic shielding, and energy storage devices due to their exceptional electronic and magnetic properties, high flexibility, and favorable hydrophilic surface, and their surface functionalities can be adjusted to various requirements [54,55]. Kim et al. [56] prepared a Ti₃C₂T_x MXene sensor via vacuum filtration method on SiO₂/Si substrate, showing a response value of 1.7% to ethanol gas, remarkable selectivity, and a ppb-level detection limit at room temperature. However, pristine MXenes suffer from shortcomings, such as relatively low sensing response and low stability under oxidative environments [57]. Therefore, MXene-based composites are being investigated to improve sensing performance. Zhang et al. [58] synthesized a MoO₃/Ti₃C₂T_x nanocomposite ethanol sensor by hydrothermal method, achieving a low-concentration limit of 1 ppm, outstanding selectivity and reproducibility, and a high response of 5.42 towards ethanol gas, which is over twice higher than the sensing response of pure MoO₃ or Ti₃C₂T_x sensors. Bu et al. [59] fabricated a Co₃O₄/Ti₃C₂T_x hybrid ethanol sensor by calcining the ZIF-67 precursor grown on the Ti₃C₂T_y sheets, demonstrating an ultra-high response (190 towards 50 ppm ethanol, which is at least 15 times higher than that of pristine Co₃O₄ or Ti₃C₂T_x sensor). Recently, the fabrication of composites (e.g., PPy/Ti₃C₂T_x)

based on ICPs and MXenes has been investigated for various applications such as supercapacitors [60], electromagnetic interference shielding [61], rechargeable batteries [62], and anticorrosive bipolar plates [63]. To the best of our knowledge, there is no previous attempt at the synthesis of PPy/Ti₃C₂T_x composites for ethanol sensing applications. It is hypothesized that combining PPy with $Ti_3C_2T_x$ might be an efficient approach for making high-performance ethanol sensors due to the synergistic effects between redox-active PPy and highly conductive $Ti_3C_2T_x$.

Henein, we developed a flexible PP/Ti $_3C_2T_x$ /PPy composite sensor by drop-coated Ti $_3C_2T_x$ MXene suspension and chemical polymerization of pyrrole on a disposable face mask (mainly made up of polypropylene (PP)) surface. The resulting sensor demonstrated excellent sensing properties. Besides, we investigated the impact of humidity, synthesis orders, bending states, and temperature on the sensing performance of the composite sensor. Finally, we designed a portable and wearable Bluetooth sensor module for detecting alcohol in human breath, indicating that the PP/Ti $_3C_2T_x$ /PPy sensor can be utilized for human drunk driving monitoring.

2. Experiment

2.1. Materials

Disposable face masks were obtained from Wenzhou Chengmu Trading Company (Wenzhou, Zhejiang, China). The polypropylene (PP) layer of the face mask is served as a substrate for the sensors. [NH₄] $_2$ S $_2$ O $_8$ (APS), and 36–38 % hydrochloric acid were purchased from Sigma-Aldrich. LiF (98.5 % purity), Ti and Al powder (325 mesh), and pyrrole monomer were purchased from Alfa Aesar. Silver paint and HF (48–51 %) were purchased from VWR, USA.

2.2. Preparation of $Ti_3C_2T_x$ solution

The Ti_3AlC_2 Max Phase and delaminated $Ti_3C_2T_x$ MXene solution were fabricated according to previous reports in the literature [54]. In summary, 1 g of Ti_3AlC_2 powder was etched in a 20 mL mixture of 12 M HCl and HF at 35 °C for 24 h. After etching, the powder was washed at least 5 times with deionized (DI) water and centrifuged at 4000 rpm for 5 min to obtain the supernatant. Afterward, the sediment was mixed with a 50 mL solution containing 1 g LiCl and stirred for 18 h. Then, the mixture was centrifuged at 4000 rpm for 5 min. The centrifuging was repeated until the dark supernatant remained. The resulting MXene solution was stored in a fridge.

2.3. Preparation of $PP/Ti_3C_2T_x$ sensor

The PP substrate was cleaned with ethanol and DI water to remove any contaminants. Then, the prepared $Ti_3C_2T_x$ MXene solution was drop-coated evenly onto the PP fabric surface. After air drying, the $Ti_3C_2T_x$ suspension was coated onto the PP surface again to synthesize the PP/Ti $_3C_2T_x$ sensor.

2.4. Preparation of PP/Ti₃C₂T_x/PPy sensor

The preparation process involved the addition of 0.6 mL pyrrole monomer to 200 mL of 1 M HCl solution in a 400 mL beaker, followed by the addition of 0.69 g of APS dissolved in 40 mL of 1 M HCl solution and then the APS-HCl solution was mixed with the pyrrole-HCl suspension at room temperature. The PP substrate and PP/Ti $_3$ C $_2$ T $_x$ were dipped in the mixed suspensions, and the polymerization reaction was performed by magnetic stirring at 30°C for 65 min. The resulting PP/PPy and PP/PP/Ti $_3$ C $_2$ T $_x$ /PPy composites were cleaned with DI water three times and dried in an oven at 40°C for 7 h. After drying, all the samples were cut into 20 mm \times 10 mm pieces. Then, the composite fabrics were coated with silver paint. Fig. 1a illustrates the synthesis process of the PP/Ti $_3$ C $_2$ T $_x$ /PPy composite sensor.

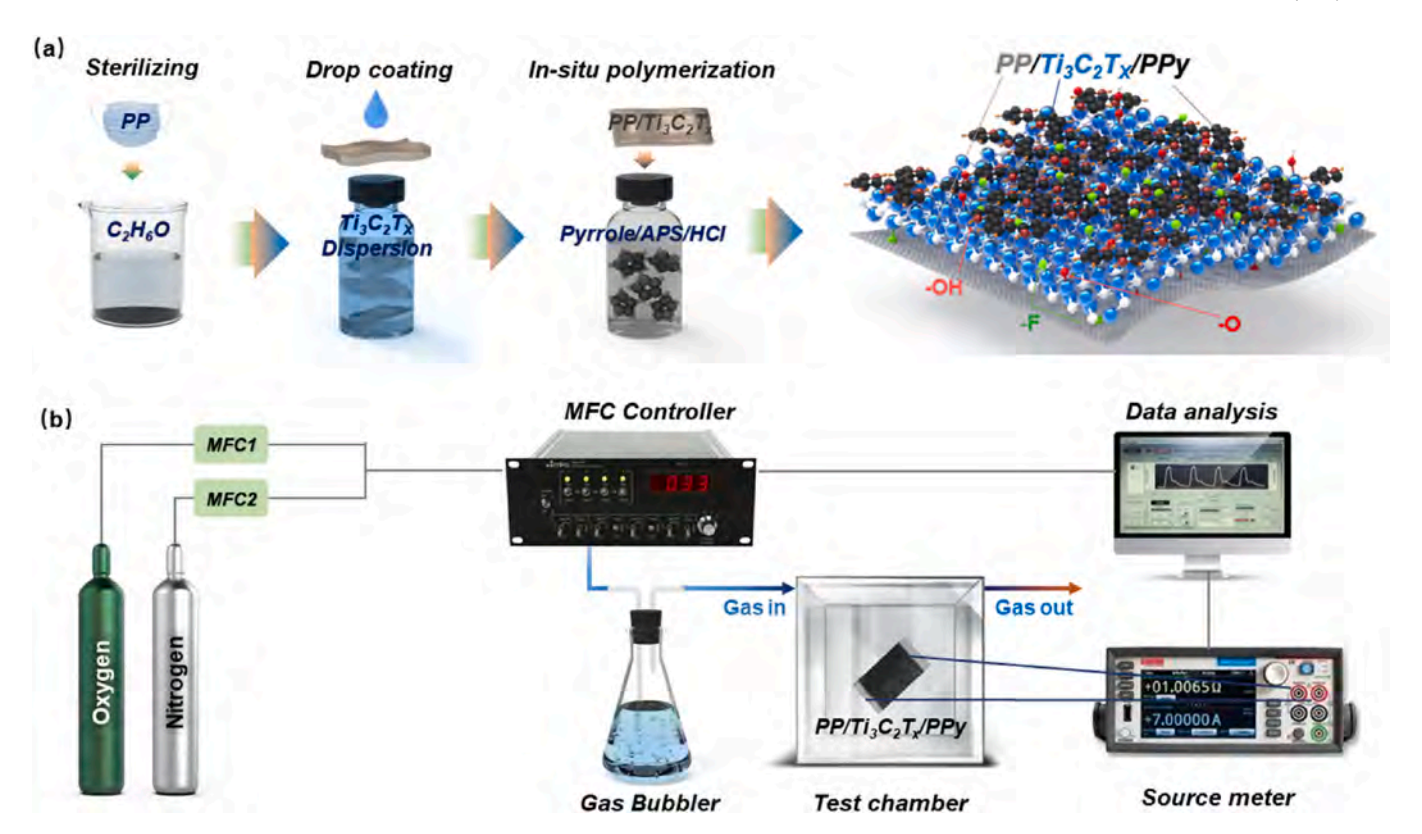


Fig. 1. (a) Schematic of the wearable PP/Ti₃C₂T_x/PPy fabric sensor synthesis process. (b) Schematic diagram of the gas sensing setup.

2.5. Sensing measurements

To investigate the sensing performance, the as-prepared samples were placed in a closed chamber and the electrical resistance change was measured by a Kethley 2400 source meter. The gas bubbling method was used to generate ethanol vapor. A flow of 80 sccm nitrogen was separated into two parts using a mass flow controller: a carrier part and a dilution part. The carrier part was bubbled through the liquid analyte of interest and then mixed with the diluted air in the test chamber. The operations were conducted at room temperature (23.5 \pm 1 $^{\circ}$ C), and the atmospheric conditions were maintained during the experiment. To control the relative humidity within the testing platform, dry synthetic air was passed through water to produce humidified air. This humidified air was then mixed with a target gas using a gas blender, with the entire system consistently maintained at room temperature. A commercial hygrometer was used throughout to monitor and ensure the desired RH values. The data collection and management were carried out using a specialized Labview program. The gas response value of the composite fabrics follows below equation:

$$R = (R_{\sigma} - R_0)/R_0 * 100\% \tag{1}$$

where R_0 and R_g are the electrical resistance of the PP/Ti $_3C_2T_x/\text{PPy}$ sensor exposed to the air and the target gas.

2.6. Wireless Bluetooth Sensor module for alcohol intoxication detection

PP/Ti $_3$ C $_2$ T $_x$ /PPy hybrid film was affixed to the surface of a disposable medical mask for alcohol breath detection. The Bluetooth sensor module was connected to the mask-sensing device, and a 5 V power bank was used to supply the voltage required by the sensor module. The resistance changes of the PP/Ti $_3$ C $_2$ T $_x$ /PPy hybrid sensor were recorded using the WeChat applet "Wireless Bluetooth Sensor" for the alcohol test. During the alcohol breath test, a volunteer drank 60 mL of whiskey (50 % ALC/VOL, 100 PROOF) and underwent alcohol breath tests at 20,

30, 40, 50, 55, 60, and 65 min, after drinking, respectively. Furthermore, the blood alcohol concentration (BAC) was determined by calibrating a commercial AD-8000 breathalyzer (2022 Upgrade Professional-Grade Accuracy Alcohol Tester, available on Amazon). After a certain duration of time since consuming alcohol, the volunteer took a deep breath and exhaled for approximately 4 s. The breathalyzer then provided the BAC value.

2.7. Characterization

The morphology and qualitative elemental analysis of the hybrid sensor were examined using a scanning electron microscope (JEOL JSM-7000F) equipped with an energy dispersive spectrometer mapping. The surface bonding of the hybrid films was investigated by FT-IR using a Thermo Nicolet 6700 instrument. Additionally, N_2 adsorption and desorption isotherms were collected to investigate the Barrett-Emmett-Teller (BET) surface area of the hybrid films. The pore size distribution of the hybrid films was analysed using the Barrett–Joyner–Halenda (BJH) method with a Quanta chrome NOVA 2200e instrument. The surface topography of the $Ti_3C_2T_x$ was characterized using an atomic force microscope (AFM, Park Instruments NX10). The valence states of elements were analysed using X-ray photoelectron spectroscopy through K-alpha (Thermo Scientific Inc., U. K.).

3. Results and discussion

3.1. Materials characterization

SEM imaging was employed to investigate the morphology of PP, PP/PPy, PP/Ti $_3C_2T_x$, and PP/Ti $_3C_2T_x$ /PPy hybrid. The PP fabric presents a straight rod-like fibrous structure, as depicted in Fig. 2a. As shown in Fig. 2b, the layered structure of $Ti_3C_2T_x$ aggregated at the PP fiber surface, indicating the successful delamination process of $Ti_3C_2T_x$. Fig. 2c clearly illustrates that the PP substrate is covered by a mass of

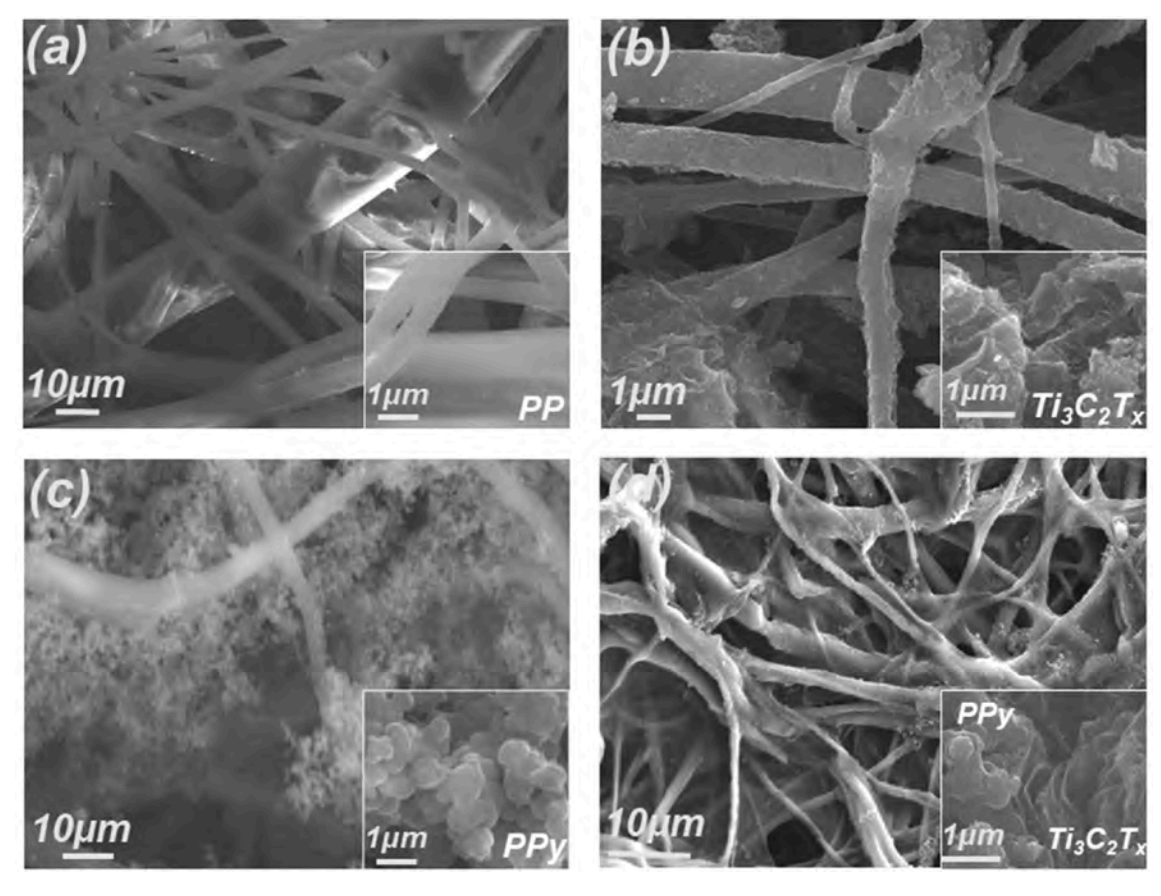


Fig. 2. SEM images of (a) PP, (b) $PP/Ti_3C_2T_x$, (c) PP/PPy, and (d) $PP/Ti_3C_2T_x/PPy$.

irregular spherical PPy particles. Additionally, Fig. 2d reveals that PPy is surrounded by some of the single-layer $Ti_3C_2T_x$, indicating that PPy was in situ polymerized on the $Ti_3C_2T_x$, and formed a well-combined structure with a porous surface, which facilitates gas adsorption and diffusion [44].

EDS mapping was conducted to investigate the surface elemental distribution in the PP/ $Ti_3C_2T_x$ /PPy hybrid, and the results are presented in Fig. 3b–h. The results revealed the presence of Cl, Ti, O, N, C, and F elements in the composite fabric. The element weight percentage and atomic percentage are presented in Fig. 3i, which further indicates the successful incorporation of PPy on the $Ti_3C_2T_x$. Fig. 3j and k show the AFM images of $Ti_3C_2T_x$, demonstrating that the delaminated $Ti_3C_2T_x$ are predominantly single layers with a thickness of 1.43 nm. The electrode structure of the PP/ $Ti_3C_2T_x$ /PPy composite sensor is illustrated in Fig. 3l. The application of silver paint on both sides of the composite sensor is to reduce contact resistance.

FT-IR was conducted to examine the surface chemistry of PP, PP/ PPy, PP/Ti₃C₂T_x, and PP/Ti₃C₂T_x/PPy, as shown in Fig. 4a. The bands at $2922\,\mathrm{cm}^{-1}, 1450\,\mathrm{cm}^{-1}, 1390\,\mathrm{cm}^{-1}, 1165\,\mathrm{cm}^{-1},$ and $842\,\mathrm{cm}^{-1}$ in PP film can be attributed to -CH2 asymmetric stretching, -CH2 symmetric bending vibration, -CH3 symmetric bending, -CH3 rocking vibration, and C-CH₃ stretching, respectively [64,65]. The peaks at 1536 cm⁻¹ 1292 cm⁻¹ in PP/PPy correspond to C=C stretching vibrations of the pyrrole ring and C-H or C-N in-plane deformation [66,67]. The absorption peaks observed at $1651~\mathrm{cm}^{-1}$, $1367~\mathrm{cm}^{-1}$, $1202~\mathrm{cm}^{-1}$, and 1002 cm⁻¹ in PP/Ti₃C₂T_v are due to C=O bonding, molecular water (O-H), oxygen group vibration and C-F vibration [68]. The intensities of the bands corresponding to -O, -OH, and -F functional groups of $Ti_3C_2T_x$ (1651, 1367, 1202, and 1002 cm⁻¹) are observed to decrease slightly in the PP/Ti₃C₂T_x/PPy, which is mainly due to the formation secondly bonding (e.g., van der Waals forces) of deposition of PPy on Ti₃C₂T_x MXene [69]. As shown in Fig. 4b, Raman shifts of the

PP/Ti $_3$ C $_2$ T $_x$ /PPy composite revealed a significant decrease in the intensity of Ti $_3$ C $_2$ T $_x$ peaks (specifically, 1316 and 1603 cm $^{-1}$ which are assigned to carbon atomic lattice defects and the stretching vibration of carbon atoms in the SP2 hybridization plane) after the PPy deposition [60]. In addition, the characteristic peaks of Ti $_3$ C $_2$ T $_x$ at 425 and 579 cm $^{-1}$ are owing to Ti–C bond vibration, and the characteristic peaks of PPy at 1356 and 1620 cm $^{-1}$ are attributed to the C–N bond stretching and C–C stretching of the pyrrole ring [70]. All these characteristic peaks indicated the successful fabrication of the PP/Ti $_3$ C $_2$ T $_x$ /PPy composite.

The XPS spectra were used to determine the surface element information and functional groups of PP/Ti₃C₂T_x and PP/Ti₃C₂T_x/PPy hybrid. The survey scan of PP/Ti₃C₂T_x and PP/Ti₃C₂T_x/PPy in Fig. 5a showed the presence of C, N, O, Ti, and F elements, indicating the combination of PPy and Ti₃C₂T_x. The C 1s signals in Fig. 5b were concentrated around 281.9, 284.3, 285.4, and 287.4 eV, which were attributed to C-Ti, C-C, C-N, and C-O/C=O, respectively. The N 1s signals in Fig. 5c were deconvoluted into three peaks centered at 398.7, 399.9, 401.9 eV, corresponding to $-N^+$, $-NH_-$, =NH, respectively. The amino groups in PPy may play an important role in promoting the formation of hydrogen bonding with ethanol molecules, which could improve the sensing performance of the composite [44]. The O 1s spectrum in Fig. 5d showed peaks at 530.1, 531.0, 532.5 eV, representing Ti-O, C-Ti-O, and Ti-OH, respectively, indicating the abundant surface terminal groups of oxygen and hydroxyl groups on the composite, these terminal groups are conducive to form hydrogen bonding with ethanol molecules to facilitate the sensing signals [60]. The high-resolution F1s spectrum in Fig. 5e showed peaks at 683.1 and 684.4 eV, ascribed to Ti-F and C-F, respectively. The Ti 2p core level in Fig. 5f was fitted with 3 different doublets (Ti 2p_{1/2} and Ti 2p_{3/2}), and the Ti 2p_{3/2} peaks at 455.2, 456.4, 458.2 eV were attributed to Ti-C, Ti²⁺/Ti³⁺, and Ti-O (Ti⁴⁺), respectively. These results suggest the partial oxidation of Ti₃C₂T_x.

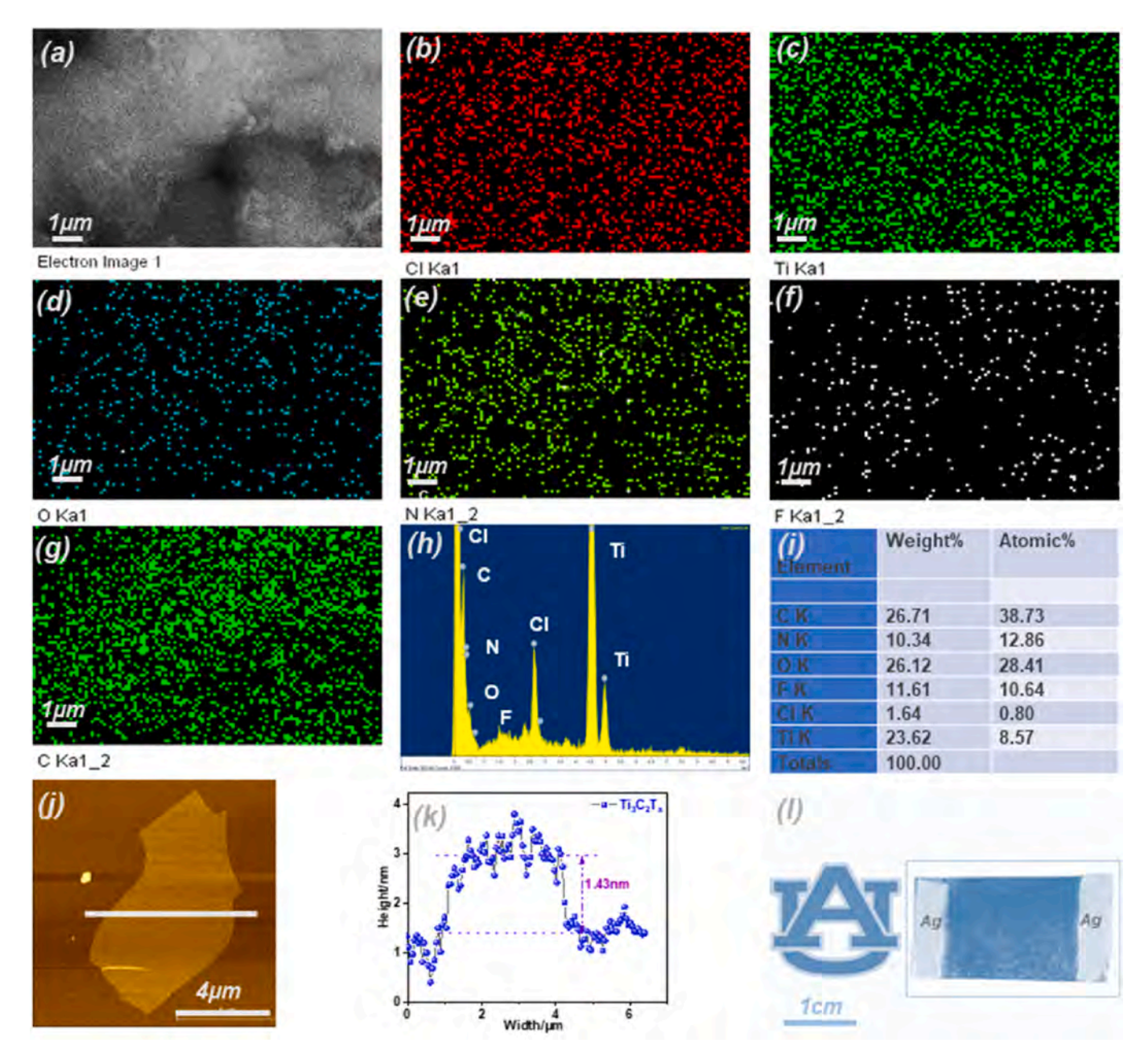


Fig. 3. Typical EDS elemental mapping of the $PP/Ti_3C_2T_x/PPy$ composite: (a) Magnified SEM image of Fig. 2d. (b–g) The distribution of Cl, Ti, O, N, C, and F elements. (h) EDS spectra of the $PP/Ti_3C_2T_x/PPy$ composite. (i) The weight and atomic percentage of each element in the $PP/Ti_3C_2T_x/PPy$ composite. (j–k) AFM image and the corresponding height and width profile of the $Ti_3C_2T_x$ flake. (l) The electrode structure of the $PP/Ti_3C_2T_x/PPy$ composite sensor.

The N_2 adsorption-desorption (BET) curves and BJH pore volume distribution as a function of the pore size are shown in Figs. S1a–d. The specific surface areas measured by the BET equation were 53.612, 60.123, 70.242, and 84.903 m² g⁻¹ for PP, PP/PPy, PP/Ti₃C₂T_x, and PP/Ti₃C₂T_x/PPy, respectively. Obviously, the PP/Ti₃C₂T_x/PPy composite displayed broader pore-size distribution with more pores and possessed the highest specific surface area among all the samples. The porous structure and the increased surface area of the PP/Ti₃C₂T_x/PPy will be beneficial to enhance sensing characteristics.

3.2. Gas-sensing properties

The sensing performance of PP/PPy, PP/ $Ti_3C_2T_x$, and PP/ $Ti_3C_2T_x$ /PPy sensors were assessed at room temperature. The resistance baseline of the PP/ $Ti_3C_2T_x$ /PPy hybrid sensor was monitored over time, ranging from 10 ppm to 400 ppm, as shown in Fig. 6a. For comparison, the

baseline resistance curves of PP/PPy and PP/Ti₃C₂T_x towards 400 ppm ethanol are shown in Fig. S2. The initial resistance of the PP/Ti₃C₂T_x/ PPy sensor was 10.5 K Ω , whereas the resistance of the PP/PPy sensor was 39.8 $K\Omega$. This indicates that adding metallic MXene significantly enhances the conductivity of the hybrid sensor. As presented in Fig. 6b, the resistance and response of all three sensors increased with the increased concentration of ethanol vapor. This might be due to the formation of more hydrogen bonds among Ti₃C₂T_x, PPy, and ethanol molecules. The sensing response of PP/PPy, PP/Ti₃C₂T_x, and PP/ Ti₃C₂T_x/PPy hybrid sensors improved as the concentration of gas increased, with the response value of 18.1 %, 35.5 %, and 76.3 % under 400 ppm ethanol, respectively. Notably, the PP/Ti₃C₂T_x/PPy hybrid sensor had a lower detection limit toward ethanol vapor (e.g., 10 ppm). The gas sensing response of PP/Ti₃C₂T_x and PP/Ti₃C₂T_x/PPy sensors as a function of concentration is presented in Fig. 6c, showing the excellent linear relationship between the sensor response and ethanol

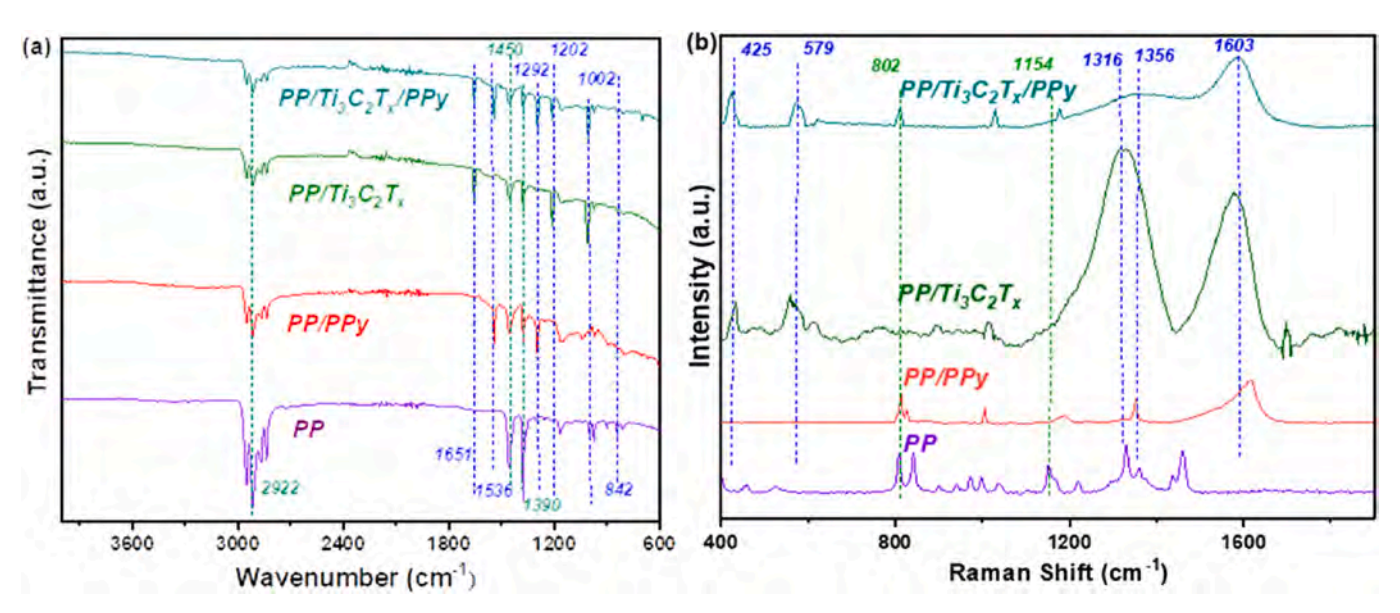
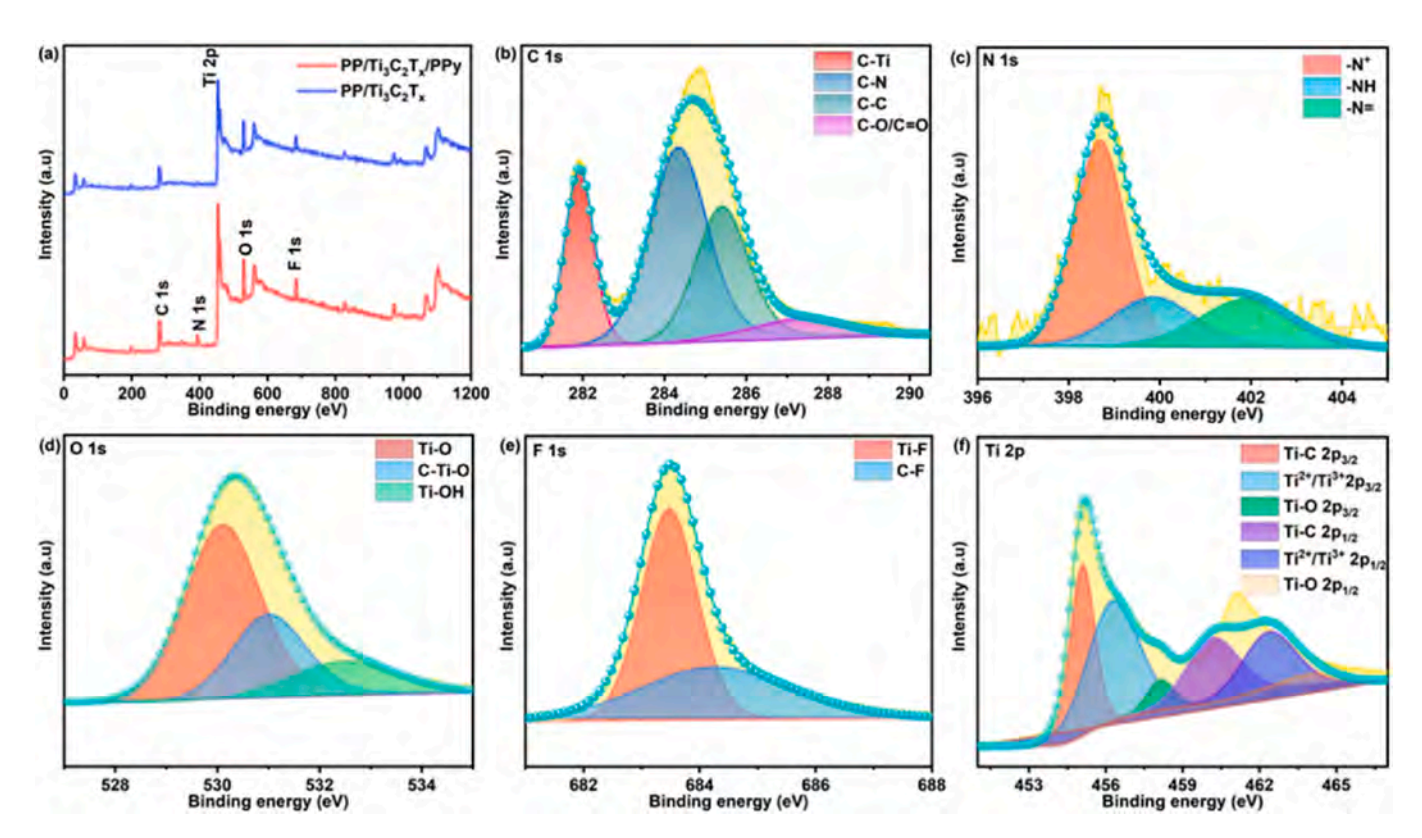


Fig. 4. (a). FTIR spectra and (b) Raman spectra of PP, PP/PPy, PP/Ti₃C₂T_x, and PP/Ti₃C₂T_x/PPy.



 $\textbf{Fig. 5.} \ \ \textbf{(a)} \ \ \textbf{The survey spectra of PP/Ti}_3 C_2 T_x \ \ \textbf{and PP/Ti}_3 C_2 T_x / PPy \ \ \textbf{hybrid.} \ \ \textbf{(b-f)} \ \ \textbf{C} \ \ \textbf{1s}, \ \textbf{N} \ \ \textbf{1s}, \ \textbf{O} \ \ \textbf{1s}, \ \textbf{F} \ \ \textbf{1s}, \ \ \textbf{and Ti} \ \ \textbf{2p} \ \ \textbf{spectra of the PP/Ti}_3 C_2 T_x / PPy \ \ \textbf{hybrid.} \ \ \textbf{N} \ \ \textbf{1s}, \ \textbf{N} \ \ \textbf{1s}, \ \textbf{O} \ \ \textbf{1s}, \ \textbf{F} \ \ \textbf{1s}, \ \ \textbf{and Ti} \ \ \textbf{2p} \ \ \textbf{spectra of the PP/Ti}_3 C_2 T_x / PPy \ \ \textbf{hybrid.} \ \ \textbf{N} \ \ \textbf{1s}, \ \ \textbf{N} \ \$

concentration. As demonstrated in Fig. 6d, the PP/ $Ti_3C_2T_x$ /PPy sensor showcased remarkable sensing capabilities. Specifically, it registered a response time of 49 s and a recovery time of 18 s. This rapidity in both response and recovery of the composite sensor can be attributed to a couple of key factors: (1) Metallic conductivity of MXene. The inherent metallic conductivity of MXene greatly enhances the conduction channels, thus effectively boosts the charge carrier transport, ensuring that the sensor reacts quickly to changes in the environment. (2) Formation of Schottky Junction [71]. Due to the Schottky barrier's sensitive nature to external changes, a small variation in the surrounding environment (such as the presence of ethanol gas) can lead to immediate changes in

the resistance. Furthermore, the impact of different synthesis orders or stacking sequence on the sensing performance was investigated, as presented in Fig. S4. The PP/PPy/Ti $_3C_2T_x$ hybrid sensor exhibited an average response value of only 50.1 %, which was much lower than that of the PP/Ti $_3C_2T_x$ /PPy sensor (76.3 %). This difference in performance can be attributed to the better dispersion conditions of the PP/Ti $_3C_2T_x$ /PPy composite, as indicated by the SEM characterization (Fig. 2b–d). The Ti $_3C_2T_x$ exhibits a uniform dispersion on the PP surface, which contributes to a higher response value of PP/Ti $_3C_2T_x$ /PPy. In contrast, PPy displays non-uniform dispersion on the PP because PPy does not wet the PP surface effectively.

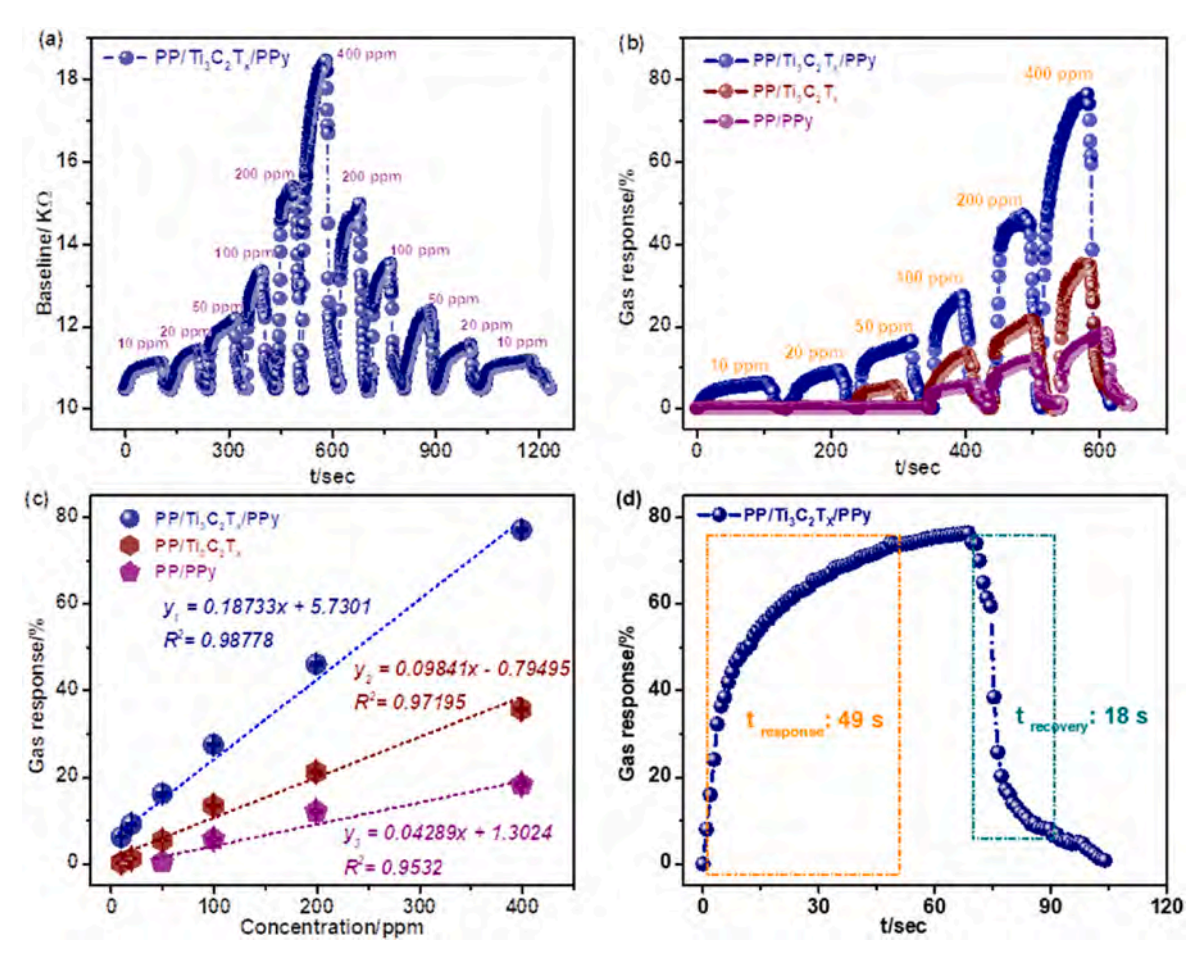


Fig. 6. (a) The real-time resistance baseline of the $PP/Ti_3C_2T_x/PPy$ hybrid sensor ranges from 10 ppm to 400 ppm. (b) The dynamic response/recovery curves of $PP/Ti_3C_2T_x$, PP/PPy, and $PP/Ti_3C_2T_x/PPy$ composite sensors. (c) Sensing response of $PP/Ti_3C_2T_x$ and $PP/Ti_3C_2T_x/PPy$ sensors as a function of ethanol concentration ranging from 10 to 400 ppm at room temperature. (d) The change of response as a function of time shows the response and recovery time. Note: the relative humidity in the test chamber was 12–18 %.

Selectivity is a vital parameter for assessing gas sensors. Therefore, the selectivity of the PP/Ti₃C₂T_x/PPy sensor was examined by comparing ethanol with various organic or inorganic gases, such as acetone, acetic acid, benzene, methane, ammonia, carbon monoxide, carbon dioxide, and hydrogen sulfide, as shown in Fig. 7a. The responses towards the above gases were 76.3 %, 25.2 %, 20.3 %, 29.4 %, 11.2 %, 38.8 %, 19.1 %, 13.0 %, and 9.2 %, respectively, implying excellent selectivity of the PP/Ti₃C₂T_x/PPy sensor towards ethanol. A primary factor contributing to this selectivity is the presence of abundant defects and functional groups like -O and -OH in Ti₃C₂T_x. These groups facilitate the absorption of ethanol gas molecules, leading to the formation of abundant hydrogen bonding. This bonding increases the binding energy, decreasing the charge carrier concentration and elevating the resistance [55]. Additionally, ethanol's interaction with PPy causes the polymer chain to swell, further enhancing the resistance [66]. The heterojunction formed between PPy and MXene (Ti₃C₂T_x) also plays a pivotal role in refining the sensor's sensing attributes. Moreover, ethanol has particular interactions with Ti₃C₂T_x or PPy, which might be stronger than interactions with other analytes. This could be due to hydrogen bonding, van der Waals forces, and/or dipole-dipole interaction [57,66]. The hydroxyl group in ethanol could be particularly prone to forming these interactions. Furthermore, the reproducibility of resistance baseline and response changes for the PP/Ti₃C₂T_x/PPy composite sensor to 400 ppm ethanol is depicted in Fig. 7b, showing the reliable reproducibility of the hybrid at room temperature. To further study the gas sensing properties of the PP/Ti₃C₂T_x/PPv hybrid, we investigated the impact of humidities, temperatures, and bending states on the sensing response. Fig. 7c displays the humidity effect on the sensing response changes of the PP/Ti₃C₂T_x/PPy composite towards 400 ppm ethanol. The sensing response of the PP/Ti₃C₂T_x/PPv composite showed an obvious decrease with the increase of humidity (15-75 % RH), i.e., the response value dropped from 76.3 % to 10.8 %. This observation might be attributed to the inhibition of the sensing reaction (e.g., hydrogen bonding) between Ti₃C₂T_x and ethanol at high humidity due to the hydrophilic nature of the Ti₃C₂T_x terminated by functional groups (e.g., -OH, -O, -F) [59]. Additionally, the presence of water molecules on the Ti₃C₂T_x/PPy active surface may lead to a decrease in gas adsorption sites, obstructing ethanol adsorption and further reducing the response [59,71]. Furthermore, the temperature effect on the response change of the PP/Ti₃C₂T_x/PPy hybrid towards 400 ppm ethanol gas ranging from 20 °C to 40 °C is presented in Fig. 7d. The PP/Ti₃C₂T_x/PPy sensor showed a slight decrease in response with the increase in temperature, which might be due to the enhanced desorption of ethanol at higher temperatures, leading to a reduction in resistance and subsequently a decrease in the sensing response [72].

The flexibility of the PP/Ti₃C₂T_x/PPy was evaluated under different bending angles towards 400 ppm ethanol gas at room temperature, and the results are shown in Fig. 8a and **b**. The response value of the PP/ $Ti_3C_2T_x$ /PPy sensor presents negligible change under different bending degrees, which demonstrates the commendable flexibility of the sensor. Besides, long-term stability is a crucial index to evaluate the reliability of the sensor. The response changes of the PP/ $Ti_3C_2T_x$ /PPy sensor towards 400 ppm ethanol at room temperature over a period of 13 days are shown in Fig. 8c and **d**. The gas response of the PP/ $Ti_3C_2T_x$ /PPy sensor

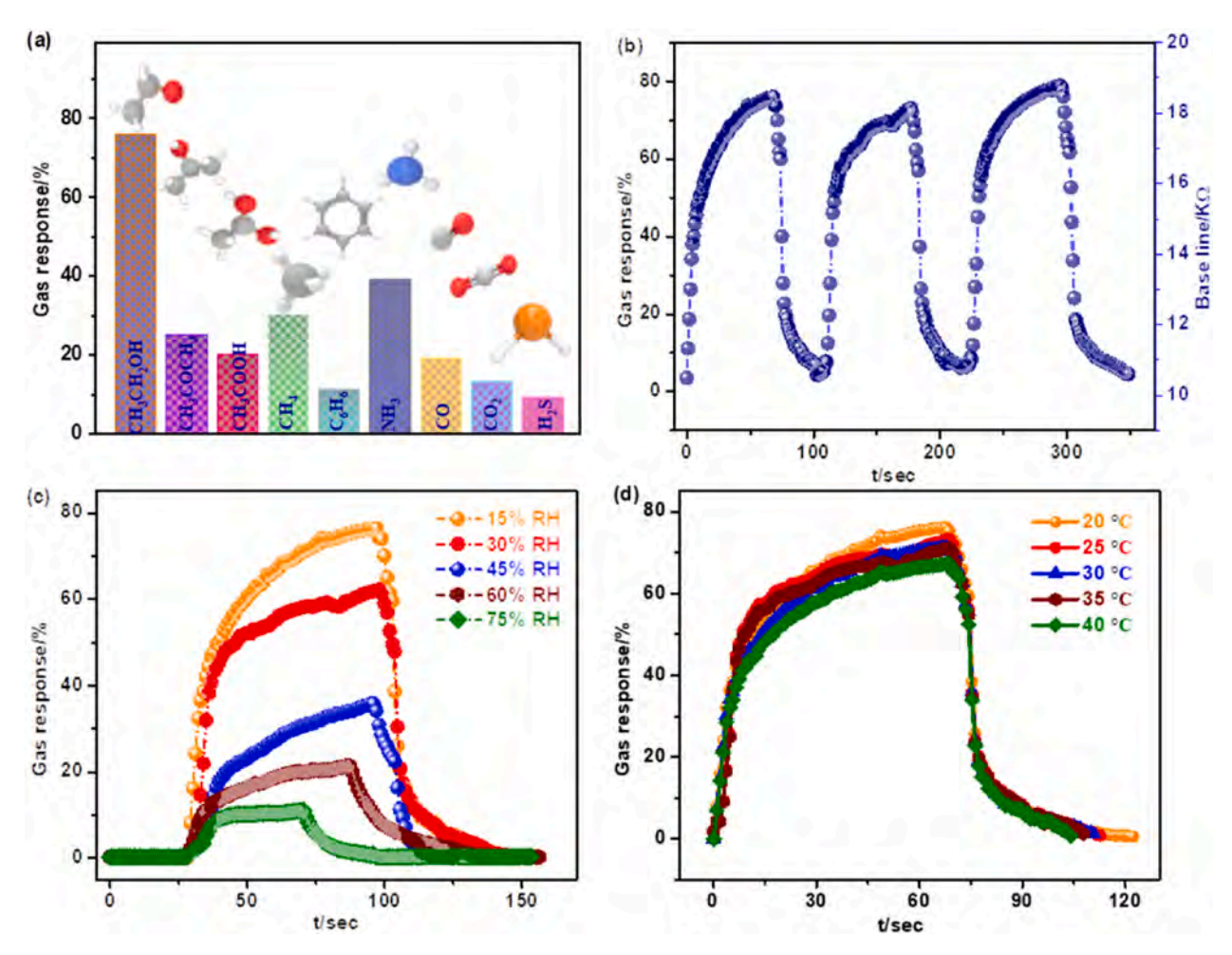


Fig. 7. (a) The selectivity study of the PP/ $Ti_3C_2T_x$ /PPy hybrid sensor to 400 ppm ethanol and other interference gases at room temperature. (b) Reproducibility cycles of resistance baseline and response changes for the PP/ $Ti_3C_2T_x$ /PPy hybrid towards 400 ppm ethanol. (c) The humidity effect on the gas response of the PP/ $Ti_3C_2T_x$ /PPy sensor under ethanol gas circumstance. (d) The temperature effect on the gas response of the PP/ $Ti_3C_2T_x$ /PPy sensor ranges from 20 °C to 40 °C.

remained above 90 % of the initial response after 13 days, indicating excellent stability of the composite sensor.

As summarized in Table 1, we compared the ethanol sensing characteristics of the sensors based on conducting polymers, Ti₃C₂T_x, or their composites in previous literature with our current work at room temperature (RT). The PP/Ti₃C₂T_x/PPy sensor exhibited a high response value, and short recovery time to ethanol gas, outperforming the sensing performance of most previously reported sensors. Moreover, Fig. S4 presents the investigation of the limit of detection (LOD) of the PP/ Ti₃C₂T_x/PPy sensor with previous studies. The result indicates that the theoretical LOD of the PP/Ti₃C₂T_v/PPy sensor (2.21 ppm) is either comparable or lower than the reported values in previous studies. The cycle stability test of the PP/Ti₃C₂T_x/PPy sensor is provided in Fig. S5. The results demonstrate notable repeatability and stability, attributed to robust interactions between PP, PPy, and MXene. These interactions include hydrogen bonding, π - π stacking, ionic bonding, van der Waals forces, among others. Besides, one of the innovative facets of our study is the utilization of face masks as substrates, which facilitates the advancement of flexible sensors and serves as a sustainable approach by addressing the ever-growing issue of mask waste. This dual-edged benefit has not been highlighted in previous literature.

3.3. The sensing mechanism of the PP/Ti₃C₂T_x/PPy sensor

Ethanol, as an electron donor molecule, can be adsorbed on the active sites of $Ti_3C_2T_x$ through dispersion forces between the partially charged surface groups and polarized ethanol molecules [55]. During

the sensing process, the bonding between ethanol molecules and terminal groups on the $Ti_3C_2T_x$ could be promoted due to the strong hydrogen bonding, leading to a higher binding energy [55,56]. This process results in the transfer of electrons from the ethanol molecules to the Ti₃C₂T_x, reducing the concentration of majority charge carriers and causing a decrease in electrical conductivity. In addition, the resistance increase of PPy towards ethanol is mainly attributed to hydrogen bonding and dipole-dipole interaction between PPy and ethanol [66]. More specifically, when PPy is exposed to ethanol, hydrogen bonding occurs between PPy and ethanol molecules, as shown in Fig. 9b. The hydrogen bonding can be understood as the dipole-dipole interaction, causing the swelling and distortion of the PPy molecular chains [66,75]. As a result, the transfer of charge carriers is negatively affected, leading to a decrease in conductivity. Besides, we used a multimeter to test the I-V characteristics of PP/Ti₃C₂T_x/PPy sensor, as shown in Fig. S6. The I-V curve for the PP/Ti₃C₂T_x/PPy composite demonstrates a non-linear relationship, suggesting the absence of an Ohmic Contact between $Ti_3C_2T_x$ and PPy.

As illustrated in Fig. 9a, the enhanced sensing performance of the $PP/Ti_3C_2T_x/PPy$ composite sensor can be explained by several synergistic effects between PPy and $Ti_3C_2T_x$. Firstly, the formation of abundant hydrogen bonds among $Ti_3C_2T_x$, PPy, and ethanol molecules enhances the binding energy of the composite and enlarges the distortion of the PPy molecular chains, thus promoting the sensing property. Secondly, numerous studies have highlighted the formation of a Schottky junction at the interface between $Ti_3C_2T_x$ and conducting polymers [71,77], as depicted in Fig. 9 (c–e). As per these findings, the

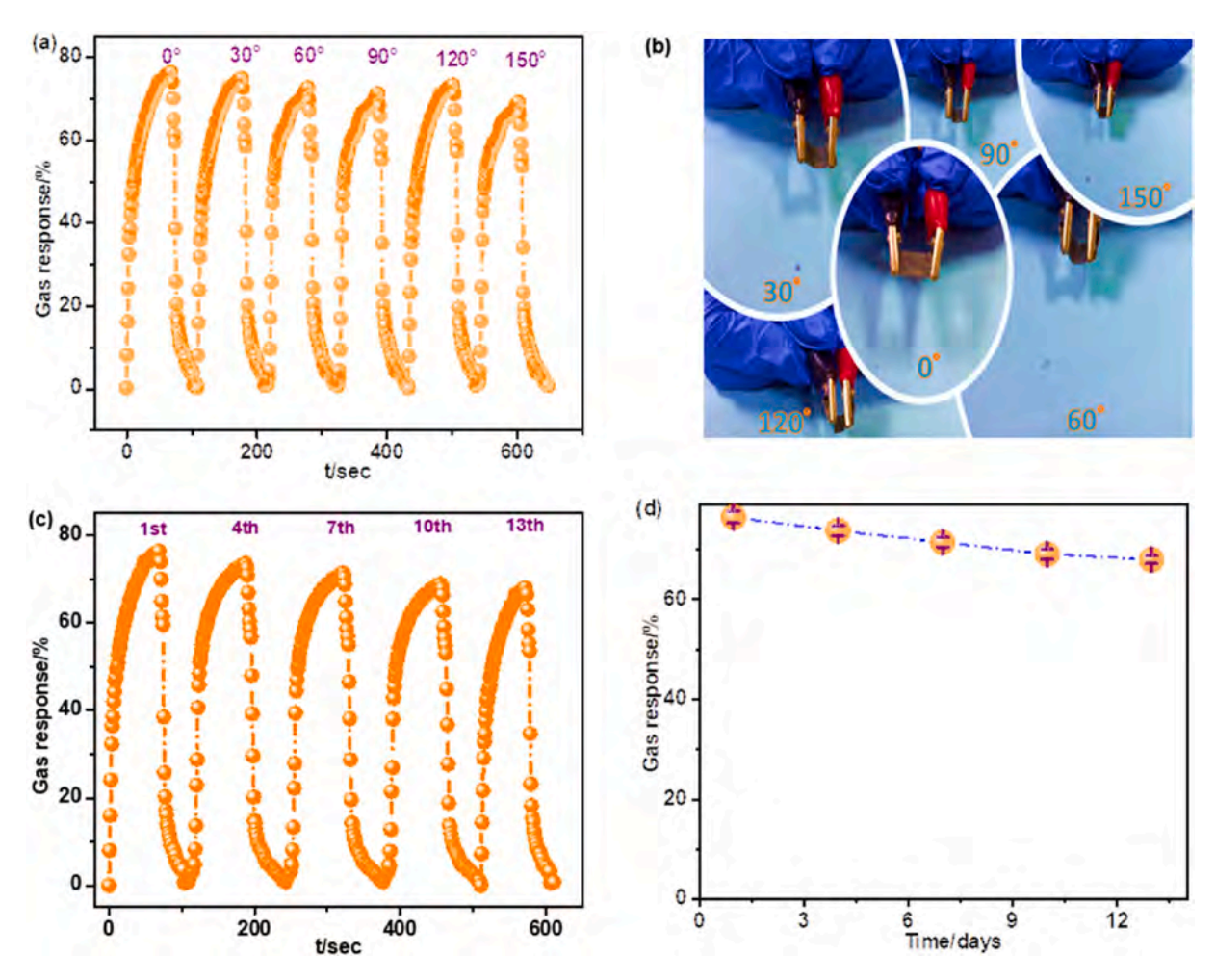


Fig. 8. (a) The response curves of the $PP/Ti_3C_2T_x/PPy$ sensor at different bending angles. (b) The different bending states of the composite sensor at 0, 30, 60, 90, 120, 150 bending angles. (c) Long-term stability of the $PP/Ti_3C_2T_x/PPy$ sensor towards 400 ppm ethanol. (d) The gas response of the $PP/Ti_3C_2T_x/PPy$ sensor as a function of time.

Table 1 Comparison of the sensing characteristics of the sensors based on conducting polymers, $Ti_3C_2T_x$, or their composites reported in the literature with the PP/ $Ti_3C_2T_x$ /PPy sensor obtained in the present work.

Sensing Materials	Substrate	Deposition Method	Analyte	Response	Response Recovery Time	Temperature	Ref
PANI/PVDF	Cu	Spin-coating	Ethanol	31.6 % (600 ppm)	50/15 s	RT	[73]
PPy nanoribbons	Glass	Coating	Ethanol	21.6 % (50 ppm)	2/31 s	RT	[66]
$Ti_3C_2T_x$	PET	Drop coating	Ethanol	11.5 % (100 ppm)	/	RT	[74]
PPy/PVA	PVA	Coating	Ethanol	70 % (100 ppm)	42/200 s	RT	[48]
$Ti_3C_2T_x$	SiO ₂ /Si	Vacuum filtration	Ethanol	1.7 % (100 ppm)	/	RT	[56]
Ti ₃ C ₂ T _x /Ag	PET	Electro-spinning	Ethanol	204 % (100 ppm)	/	RT	[6]
Ti ₃ C ₂ T _x /PPy	PP	Drop-coating	Ethanol	76.3 % (400 ppm)	49/18 s	RT	This work

UPS results indicate the work function of $Ti_3C_2T_x$ to be 4.31 eV [71], and the PPy's work function ranging between 4.6 and 5.2 eV [76]. This disparity suggests a directionality to the electron transfer from $Ti_3C_2T_x$ to PPy, while hole transfer occurs in the reverse direction, from PPy to $Ti_3C_2T_x$. Such interactions lead to the creation of a Schottky junction at the interface, resulting in a narrowed hole depletion layer [77]. During the gas sensing activity, PPy absorbs ethanol molecules, which in turn decreases the concentration of holes (polarons). This event causes an expansion of the depletion region at the composite interface, which subsequently enhances the sensing characteristics. Additionally, a p-n junction may form between the n-type of TiO_2 (due to the partial oxidation of $Ti_3C_2T_x$) and PPy at the composite interface to improve sensing properties [77]. Furthermore, the excellent conductivity of $Ti_3C_2T_x$ promotes the electron transport process of the PP/ $Ti_3C_2T_x$ /PPy

composite, and the abundant surface functional groups (such as -OH, -O) on $Ti_3C_2T_x$ expand the connecting channels for gas diffusion, thereby facilitating the sensing property [74]. Finally, the porous and uniform structure of the $PP/Ti_3C_2T_x/PPy$ composite, with a specific surface area of $84.9~\text{m}^2/\text{g}$, provides a larger number of adsorption sites on the composite surface, improving the adsorption process of ethanol gas molecules and thus promoting the sensing performance [77].

Furthermore, FTIR analysis reveals a subtle reduction in the -O, -OH, and -F functional groups of $Ti_3C_2T_x$ within the $PP/Ti_3C_2T_x/PPy$ composite. This indicates a potential influence on the $Ti_3C_2T_x$, which stands as a primary material for ethanol sensing. This change can be largely attributed to the secondary bonding resulting from the dispersion of PPy on the $Ti_3C_2T_x$ MXene. Interestingly, even with this reduction of functional groups, there's an observable enhancement in sensing

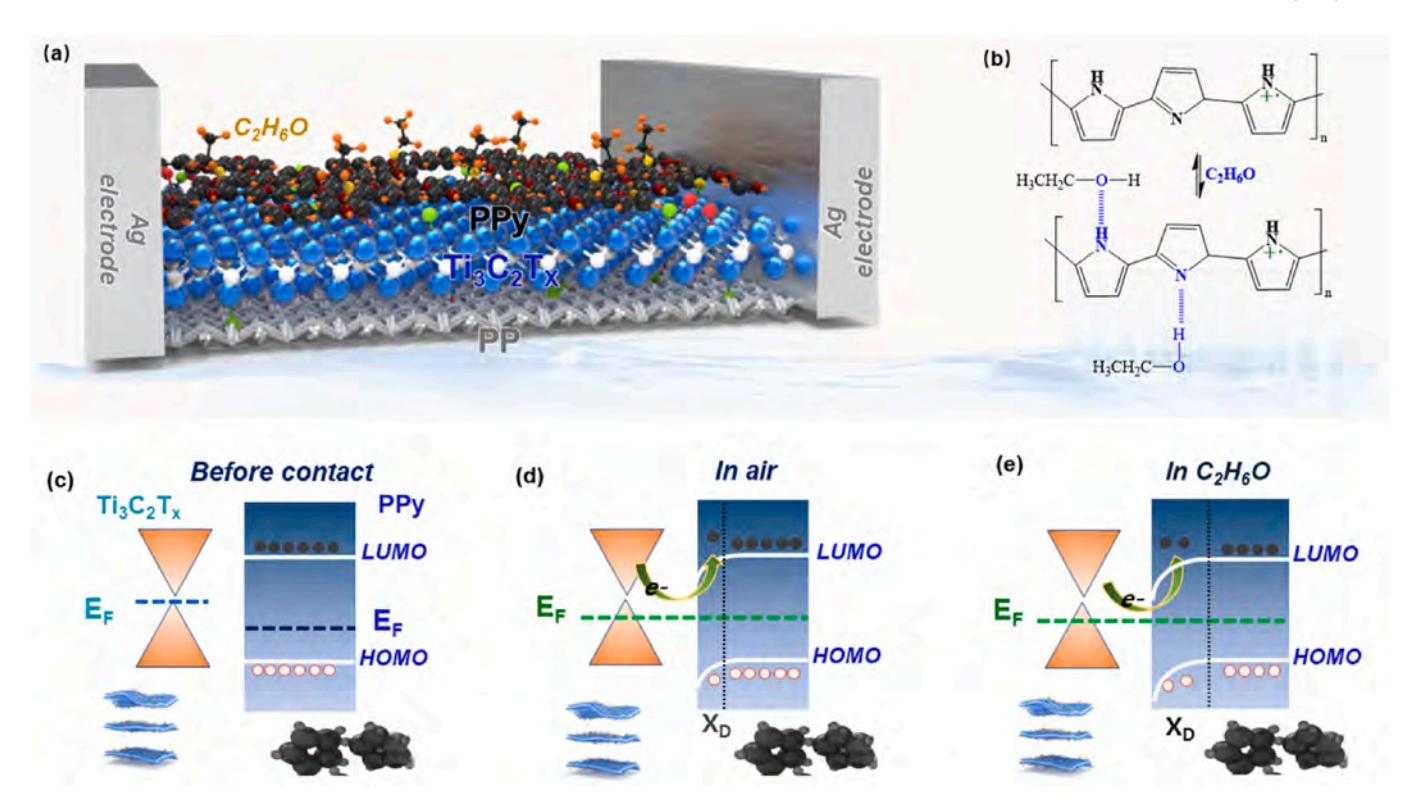


Fig. 9. (a). The proposed sensing mechanism of the $PP/Ti_3C_2T_x/PPy$ sensor towards ethanol gas. (b) The hydrogen bonding interaction between PPy and ethanol molecules. (c–e). The band structure between PPy and $Ti_3C_2T_x$: (c) before contact, (d) contact and the formation of Schottky junction in air, and (e) in ethanol, X_D is the width of the hole depletion layer.

performance upon integrating PPy with $Ti_3C_2T_x$. We believe this enhancement can be credited to the dominant role of the Schottky junction in ethanol sensing. The increased number of charge carriers, improved charge transfer, and expanded depletion layer width appear to compensate for the drawbacks seen due to the decreased functional groups post the PPy combination with $Ti_3C_2T_x$. Notably, such an observation remains unreported in existing literature.

3.4. Bluetooth sensor module for alcohol exhaled breath monitoring

In the United States, driving with a blood alcohol concentration (BAC) level above 0.08 % is considered a criminal offense. To monitor BAC levels for drunk driving, we developed a wearable Bluetooth sensor module by integrating the $PP/Ti_3C_2T_x/PPy$ composite into a disposable face mask, as shown in Fig. 10(a-d). We compared the alcohol sensing performance of our Bluetooth sensor module with a commercial AD-8000 Breathalyzer and plotted the results for BAC levels ranging from 0 to 0.19 % in Fig. 10(e-k) and Videos S (1-8). The PP/Ti₃C₂T_x/PPy composite showed sensing responses of -3.3%, 4.7%, 10.6%, 24.7%, 35.4 %, 71.4 %, and 102.1 % to BAC levels of 0 %, 0.013 %, 0.022 %, 0.051 %, 0.084 %, 0.145 %, and 0.190 %, respectively. We observed that the BAC detection was mainly dependent on the concentration of alcohol and the moisture in exhaled breath, while temperature and bending states had little influence on the alcohol sensing property. The negative sensing signals in Fig. 10e were mainly due to the high humidity in the exhaled gas, which led to the proton effect on the composite sensor, causing the resistance decrease [78]. Additionally, the higher the BAC concentration, the stronger the response intensity observed by the portable Bluetooth sensor module. Moreover, the concentration of alcohol in exhaled breath decreases continuously with time, resulting in weaker signal intensities towards the end of the curves. Interestingly, we observed an outstanding linear relationship between the BAC detected by the commercial Breathalyzer and the alcohol response tested by our Bluetooth sensor module, as shown in Fig. 10l.

Furthermore, we conducted a 5-min maintenance test of the $PP/Ti_3C_2T_x/PPy$ composite sensor towards 0.084 % BAC, which proved the reliable stability of our wireless sensing module, as depicted in Fig. 10m. These results indicate that our as-designed wireless sensing module device can be used for real-time alcohol breath monitoring, demonstrating its potential as a breath analyzer for human drunk driving monitoring.

4. Conclusion

In this study, we developed a wearable PP/Ti₃C₂T_x/PPy composite sensor by combining delaminated Ti₃C₂T_x MXene and PPy on a disposable face mask. The composite sensor depicted a rapid response (49s) and recovery time (18s), excellent repeatability and selectivity, low theoretical limit of detection (2.22 ppm), and a high response value of 76.3 % towards 400 ppm ethanol gas, with a sensing response value above 69 % even after 13 days. Meanwhile, we observed a negative effect of humidity on the sensing performance due to obstructed ethanol adsorption and decreased gas adsorption sites. Moreover, we elucidated the mechanism for the enhanced sensing property, which was attributed to the abundant functional groups on the composite and the formation of the Schottky junction between Ti₃C₂T_x and PPy. Additionally, we demonstrated a wearable wireless Bluetooth sensing module based on the PP/Ti₃C₂T_v/PPv composite, which could detect different alcohol concentrations in human breath at room temperature. It is believed that the PP/Ti₃C₂T_x/PPy composite sensor has great potential for practical applications in human drunk driving monitoring.

CRediT authorship contribution statement

Guodong Wu: Conceptualization, Investigation, Data curation, Writing – original draft. **Haishun Du:** Conceptualization, Investigation, Writing – original draft. **Kiandokht Pakravan:** Data curation, Writing – review & editing. **Wonhyeong Kim:** Data curation, Writing – review &

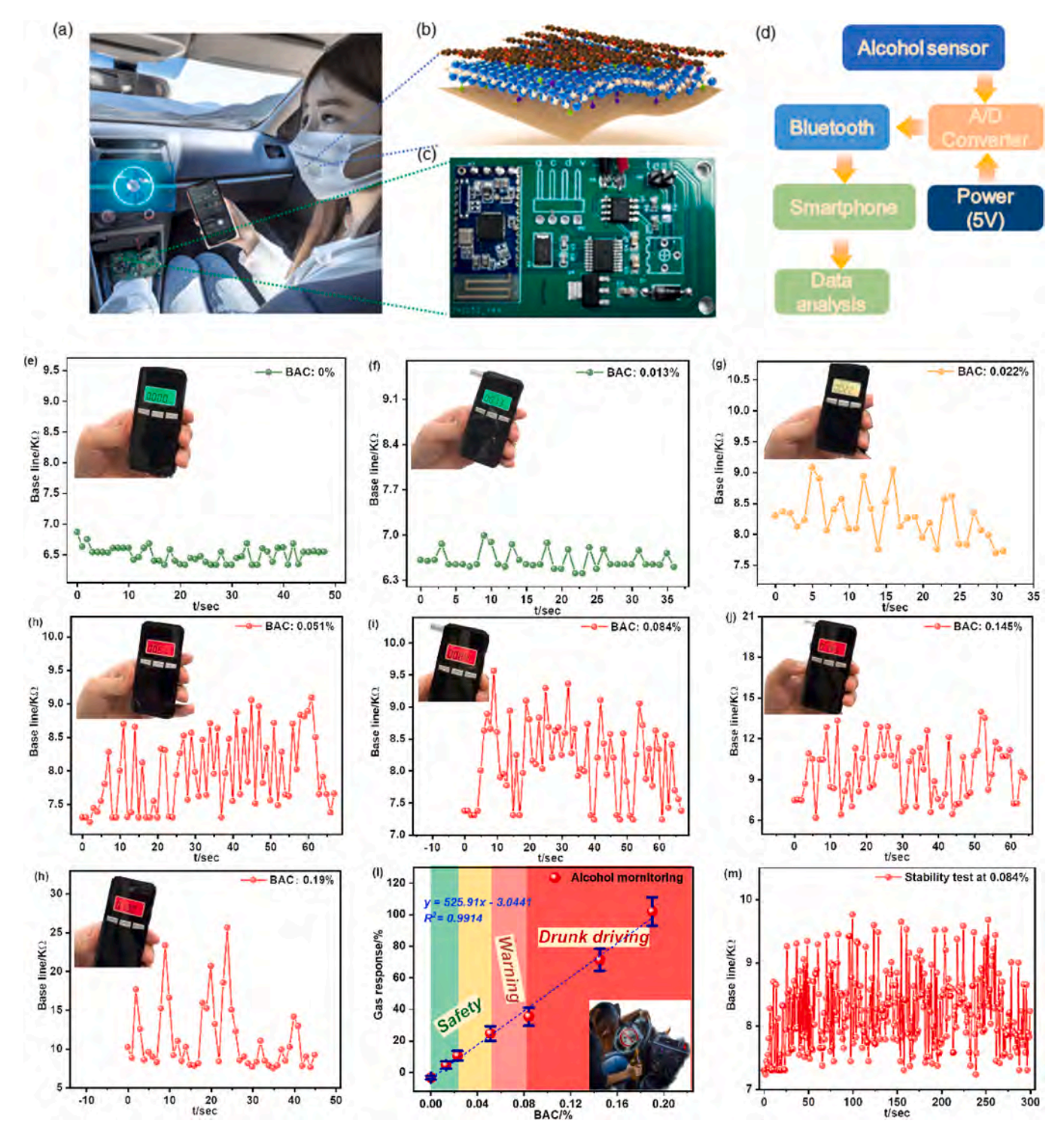


Fig. 10. (a) Schematic of flexible $PP/Ti_3C_2T_x/PPy$ -based wearable Bluetooth sensor module device for alcohol breath detection. (b) The $PP/Ti_3C_2T_x/PPy$ composite. (c) The wireless Bluetooth sensor module. (d). The $PP/Ti_3C_2T_x/PPy$ hybrid was utilized as an alcohol breath sensor and connected to a readout circuit (Fig. S7) that was powered by a 5V voltage source. The signals generated by the sensor were then transmitted via Bluetooth to a smartphone. (e–k) The alcohol exhaled breath test under different BAC. (l) The curve that fits the gas response to BAC. (m) The alcohol breath stability test.

editing. **Yoo Lim Cha:** Data curation. **Majid Beidaghi:** Writing – review & editing. **Xinyu Zhang:** Writing – review & editing. **Xuejun Pan:** Writing – review & editing. **Dong-Joo Kim:** Conceptualization, Investigation, Supervision, Funding acquisition, Writing – review & editing.

Declaration of competing interest

The authors declare that they have no known competing financial interests or personal relationships that could have appeared to influence the work reported in this paper.

Acknowledgments

G. Wu acknowledges the financial support from the China Scholarship Council (No. 201908370203). K. Pakravan and M. Beidaghi acknowledge support from National Science Foundation under Award No. 1944680.

Appendix A. Supplementary data

Supplementary data to this article can be found online at https://doi. org/10.1016/j.carbon.2023.118565.

References

- J. van den Broek, S. Abegg, S.E. Pratsinis, A.T. Güntner, Highly selective detection of methanol over ethanol by a handheld gas sensor, Nat. Commun. 10 (1) (2019) 4220
- [2] Y. Ravi Kumar, K. Deshmukh, T. Kovářík, S.K. Khadheer Pasha, A systematic review on 2D materials for volatile organic compound sensing, Coord. Chem. Rev. 461 (2022), 214502.
- [3] W.Y. Chen, X. Jiang, S.-N. Lai, D. Peroulis, L. Stanciu, Nanohybrids of a MXene and transition metal dichalcogenide for selective detection of volatile organic compounds, Nat. Commun. 11 (1) (2020) 1302.
- [4] K.M. Tripathi, T. Kim, D. Losic, T.T. Tung, Recent advances in engineered graphene and composites for detection of volatile organic compounds (VOCs) and noninvasive diseases diagnosis, Carbon 110 (2016) 97–129.
- [5] S. He, W. Li, L. Feng, W. Yang, Rational interaction between the aimed gas and oxide surfaces enabling high-performance sensor: the case of acidic α-MoO₃ nanorods for selective detection of triethylamine, J. Alloys Compd. 783 (2019) 574–582.
- [6] W. Yuan, K. Yang, H. Peng, F. Li, F. Yin, A flexible VOCs sensor based on a 3D Mxene framework with a high sensing performance, J. Mater. Chem. A 6 (37) (2018) 18116–18124.
- [7] S. Chatterjee, M. Castro, J.F. Feller, Tailoring selectivity of sprayed carbon nanotube sensors (CNT) towards volatile organic compounds (VOC) with surfactants, Sensor. Actuator. B Chem. 220 (2015) 840–849.
- [8] Y. Adiguzel, H. Kulah, Breath sensors for lung cancer diagnosis, Biosens. Bioelectron. 65 (2015) 121–138.
- [9] K. Zhang, S. Qin, P. Tang, Y. Feng, D. Li, Ultra-sensitive ethanol gas sensors based on nanosheet-assembled hierarchical ZnO-In2O₃ heterostructures, J. Hazard Mater. 391 (2020), 122191.
- [10] L. Wang, Y. Kang, X. Liu, S. Zhang, W. Huang, S. Wang, ZnO nanorod gas sensor for ethanol detection, Sensor. Actuator. B Chem. 162 (1) (2012) 237–243.
- [11] P. Azimi, D. Zhao, C. Pouzet, N.E. Crain, B. Stephens, Emissions of ultrafine particles and volatile organic compounds from commercially available desktop three-dimensional printers with multiple filaments, Environ. Sci. Technol. 50 (3) (2016) 1260–1268.
- [12] A.T. Ubando, A.D.M. Africa, M.C. Maniquiz-Redillas, A.B. Culaba, W.-H. Chen, Reduction of particulate matter and volatile organic compounds in biorefineries: a state-of-the-art review, J. Hazard Mater. 403 (2021), 123955.
- [13] A. Mirzaei, S. Park, G.-J. Sun, H. Kheel, C. Lee, S. Lee, Fe₂O₃/Co₃O₄ composite nanoparticle ethanol sensor, J. Kor. Phys. Soc. 69 (3) (2016) 373–380.
- [14] S. Choi, M. Bonyani, G.-J. Sun, J.K. Lee, S.K. Hyun, C. Lee, Cr₂O₃ nanoparticle-functionalized WO₃ nanorods for ethanol gas sensors, Appl. Surf. Sci. 432 (2018) 241–240
- [15] Z.-g. Li, Comparative study on WHO western pacific region and world federation of Chinese medicine societies international standard terminologies on traditional medicine: diseases of paediatrics (Part 1), J. Integr. Med. 13 (1) (2015) 61–64.
- [16] B.H. Ghassan, L. Francine, J.C. Aaron, R.-N. Ole, B. Michael, L. Dana, Lung cancer and exposure to nitrogen dioxide and traffic: a systematic review and metaanalysis, Environ. Health Perspect. 123 (11) (2015) 1107–1112.
- [17] K. Ram, M. Sarin, A. Sudheer, R. Rengarajan, Carbonaceous and secondary inorganic aerosols during wintertime fog and haze over urban sites in the Indo-Gangetic Plain, Aerosol Air Qual. Res. 12 (3) (2012) 359–370.
- [18] C. Chen, K.D. Campbell, I. Negi, R.A. Iglesias, P. Owens, N. Tao, F. Tsow, E. S. Forzani, A new sensor for the assessment of personal exposure to volatile organic compounds, Atmos. Environ. 54 (2012) 679–687.
- [19] L. Spinelle, M. Gerboles, G. Kok, S. Persijn, T. Sauerwald, Review of portable and low-cost sensors for the ambient air monitoring of benzene and other volatile organic compounds, Sensors-Basel 17 (7) (2017) 1520.
- [20] A. Williams, I. Altman, D. Burnett, E. Gutierrez Zorrilla, A.R. Garcia, C. Cagle, C. Luke Croessmann, M. Pantoya, Variations in aluminum particle surface energy and reactivity induced by annealing and quenching, Appl. Surf. Sci. 579 (2022), 152185.
- [21] W.-C. Chiang, C.-Y. Chen, T.-C. Lee, H.-L. Lee, Y.-W. Lin, Fast and simple screening for the simultaneous analysis of seven metabolites derived from five volatile organic compounds in human urine using on-line solid-phase extraction coupled with liquid chromatography-tandem mass spectrometry, Talanta 132 (2015) 469–478.
- [22] F. Haghighi, Z. Talebpour, A. Sanati-Nezhad, Through the years with on-a-chip gas chromatography: a review, Lab Chip 15 (12) (2015) 2559–2575.

[23] A. Kumar, J. Brunet, C. Varenne, A. Ndiaye, A. Pauly, Phthalocyanines based QCM sensors for aromatic hydrocarbons monitoring: role of metal atoms and substituents on response to toluene, Sensor. Actuator. B Chem. 230 (2016) 320, 320.

- [24] H. Jung, H. Min, J. Hwang, J. Kim, Y.-S. Choe, H.-S. Lee, W. Lee, Selective detection of sub-1-ppb level isoprene using Pd-coated In₂O₃ thin film integrated in portable gas chromatography, Appl. Surf. Sci. 586 (2022), 152827.
- [25] M. Righettoni, A. Amann, S.E. Pratsinis, Breath analysis by nanostructured metal oxides as chemo-resistive gas sensors, Mater. Today 18 (3) (2015) 163–171.
- [26] B. Si, E. Song, Recent advances in the detection of neurotransmitters, Chemosensors 6 (1) (2018) 1.
- [27] X. Xiao, X. Zhou, J. Ma, Y. Zhu, X. Cheng, W. Luo, Y. Deng, Rational synthesis and gas sensing performance of ordered mesoporous semiconducting WO₃/NiO composites, ACS Appl. Mater. Interfaces 11 (29) (2019) 26268–26276.
- [28] N.B. Tanvir, O. Yurchenko, E. Laubender, G. Urban, Investigation of low temperature effects on work function based CO₂ gas sensing of nanoparticulate CuO films, Sensor. Actuator. B Chem. 247 (2017) 968–974.
- [29] W.-Y. Li, L.-N. Xu, J. Chen, Co₃O₄ nanomaterials in lithium-ion batteries and gas sensors, Adv. Funct. Mater. 15 (5) (2005) 851–857.
- [30] D. Fu, C. Zhu, X. Zhang, C. Li, Y. Chen, Two-dimensional net-like SnO₂/ZnO heteronanostructures for high-performance H₂ S gas sensor, J. Mater. Chem. A 4 (4) (2016) 1390–1398.
- [31] S. Chang, M. Yang, R. Pang, L. Ye, X. Wang, A. Cao, Y. Shang, Intrinsically flexible CNT-TiO₂-Interlaced film for NO sensing at room temperature, Appl. Surf. Sci. 579 (2022), 152172.
- [32] N. Li, Y. Fan, Y. Shi, Q. Xiang, X. Wang, J. Xu, A low temperature formaldehyde gas sensor based on hierarchical SnO/SnO₂ nano-flowers assembled from ultrathin nanosheets: synthesis, sensing performance and mechanism, Sensor. Actuator. B Chem. 294 (2019) 106–115.
- [33] C.R. Michel, A.H. Martínez-Preciado, E.R. López-Mena, A. Elías-Zuñiga, N. Cayetano-Castro, O. Ceballos-Sanchez, Improvement of the gas sensing response of nanostructured LaCoO₃ by the addition of Ag nanoparticles, Sensor. Actuator. B Chem. 246 (2017) 181–189.
- [34] H. Iwakuni, Y. Shinmyou, H. Yano, H. Matsumoto, T. Ishihara, Direct decomposition of NO into N₂ and O₂ on BaMnO₃-based perovskite oxides, Appl. Catal. B Environ. 74 (3–4) (2007) 299–306.
- [35] A.S. Zoolfakar, M.Z. Ahmad, R.A. Rani, J.Z. Ou, S. Balendhran, S. Zhuiykov, K. Latham, W. Wlodarski, K. Kalantar-zadeh, Nanostructured copper oxides as ethanol vapour sensors, Sensor. Actuator. B Chem. 185 (2013) 620–627.
- [36] W. Qin, Z. Yuan, H. Gao, R. Zhang, F. Meng, Perovskite-structured LaCoO₃ modified ZnO gas sensor and investigation on its gas sensing mechanism by first principle, Sensor. Actuator. B Chem. 341 (2021), 130015.
- [37] G. Atanasova, A.O. Dikovska, T. Dilova, B. Georgieva, G.V. Avdeev, P. Stefanov, N. N. Nedyalkov, Metal-oxide nanostructures produced by PLD in open air for gas sensor applications, Appl. Surf. Sci. 470 (2019) 861–869.
- [38] U.T. Nakate, P. Patil, Y.T. Nakate, S.-I. Na, Y.T. Yu, Y.-B. Hahn, Ultrathin ternary metal oxide Bi₂MoO₆ nanosheets for high performance asymmetric supercapacitor and gas sensor applications, Appl. Surf. Sci. 551 (2021), 149422.
- [39] I.S. Jeon, G. Bae, M. Jang, Y. Yoon, S. Jang, W. Song, S. Myung, J. Lim, S.S. Lee, H.-K. Jung, J. Hwang, K.-S. An, Atomic-level mediation in structural interparameter tradeoff of zinc oxide nanowires-based gas sensors: ZnO nanofilm/ZnO nanowire homojunction array, Appl. Surf. Sci. 540 (2021), 148350.
- [40] Y.K. Jo, S.-Y. Jeong, Y.K. Moon, Y.-M. Jo, J.-W. Yoon, J.-H. Lee, Exclusive and ultrasensitive detection of formaldehyde at room temperature using a flexible and monolithic chemiresistive sensor, Nat. Commun. 12 (1) (2021) 4955.
- [41] S. Nakata, M. Shiomi, Y. Fujita, T. Arie, S. Akita, K. Takei, A wearable pH sensor with high sensitivity based on a flexible charge-coupled device, Nature Electronics 1 (11) (2018) 596–603.
- [42] G. Wu, H. Du, Y.L. Cha, D. Lee, W. Kim, F. Feyzbar-Khalkhali-Nejad, T.-S. Oh, X. Zhang, D.-J. Kim, A wearable mask sensor based on polyaniline/CNT nanocomposites for monitoring ammonia gas and human breathing, Sensor. Actuator. B Chem. 375 (2023), 132858.
- [43] G. Wu, H. Du, D. Lee, Y.L. Cha, W. Kim, X. Zhang, D.-J. Kim, Polyaniline/graphene-Functionalized flexible waste mask sensors for ammonia and volatile sulfur compound monitoring, ACS Appl. Mater. Interfaces 14 (50) (2022) 56056–56064.
- [44] X. Wen, Y. Cai, X. Nie, J. Xiong, Y. Wang, H. Song, Z. Li, Y. Shen, C. Li, PSS-doped PANI nanoparticle/Ti₃C₂T_x composites for conductometric flexible ammonia gas sensors operated at room temperature, Sensor. Actuator. B Chem. 374 (2023), 132788
- [45] H. He, M. Zhang, T. Zhao, H. Zeng, L. Xing, X. Xue, A self-powered gas sensor based on PDMS/Ppy triboelectric-gas-sensing arrays for the real-time monitoring of automotive exhaust gas at room temperature, Sci. China Mater. 62 (2095–8226) (2019) 1433.
- [46] S.S. Barkade, J.B. Naik, S.H. Sonawane, Ultrasound assisted miniemulsion synthesis of polyaniline/Ag nanocomposite and its application for ethanol vapor sensing, Colloids Surf. A Physicochem. Eng. Asp. 378 (1–3) (2011) 94–98.
- [47] I. Gawri, R. Ridhi, K. Singh, S. Tripathi, Chemically synthesized TiO₂ and PANI/ TiO₂ thin films for ethanol sensing applications, Mater. Res. Express 5 (2) (2018), 025303.
- [48] M. Das, D. Sarkar, Development of room temperature ethanol sensor from polypyrrole (PPy) embedded in polyvinyl alcohol (PVA) matrix, Polym. Bull. 75 (2018) 3109–3125.
- [49] P. Sajad, H. Heidari, Soft polymerization of polypyrrole-ZnO and polypyrrole-V₂O₅ nanocomposites and their application as selective gas sensor, Sens. Lett. 15 (1) (2017) 19–24.

- [50] S.M. Yenorkar, R.N. Zade, B.M. Mude, V.M. Mayekar, K.M. Mude, K.B. Raulkar, R. R. Mistry, A. Patange, Polymer-Metal Oxide Composite (PPy-MoO₃) for Ammonia and Ethanol Gas Sensor, Macromolecular Symposia, Wiley Online Library, 2021, 2100049
- [51] V.S. Bhati, M. Kumar, R. Banerjee, Gas sensing performance of 2D nanomaterials/ metal oxide nanocomposites: a review, J. Mater. Chem. C. 9 (28) (2021) 8776–8808
- [52] W. Choi, J. Kim, E. Lee, G. Mehta, V. Prasad, Asymmetric 2D MoS₂ for scalable and high-performance piezoelectric sensors, ACS Appl. Mater. Interfaces 13 (11) (2021) 13596–13603.
- [53] A.V. Agrawal, N. Kumar, M. Kumar, Strategy and future prospects to develop room-temperature-recoverable NO₂ gas sensor based on two-dimensional molybdenum disulfide, Nano-Micro Lett. 13 (2021) 1–58.
- [54] A. VahidMohammadi, J. Rosen, Y. Gogotsi, The world of two-dimensional carbides and nitrides (MXenes), Science 372 (6547) (2021), eabf1581.
- [55] E. Lee, A. VahidMohammadi, B.C. Prorok, Y.S. Yoon, M. Beidaghi, D.-J. Kim, Room temperature gas sensing of two-dimensional titanium carbide (MXene), ACS Appl. Mater. Interfaces 9 (42) (2017) 37184–37190.
- [56] S.J. Kim, H.-J. Koh, C.E. Ren, O. Kwon, K. Maleski, S.-Y. Cho, B. Anasori, C.-K. Kim, Y.-K. Choi, J. Kim, Y. Gogotsi, H.-T. Jung, Metallic Ti3C2Tx MXene gas sensors with ultrahigh signal-to-noise ratio, ACS Nano 12 (2) (2018) 986–993.
- [57] Y. Pei, X. Zhang, Z. Hui, J. Zhou, X. Huang, G. Sun, W. Huang, Ti₃C₂T_x MXene for sensing applications: recent progress, design principles, and future perspectives, ACS Nano 15 (3) (2021) 3996–4017.
- [58] S. Zhang, P. Song, J. Sun, Y. Ding, Q. Wang, MoO₃/Ti₃C₂T_x MXene nanocomposites with rapid response for enhanced ethanol-sensing at a low temperature, Sensor. Actuator. B Chem. 378 (2023), 133216.
- [59] X. Bu, F. Ma, Q. Wu, H. Wu, Y. Yuan, L. Hu, C. Han, X. Wang, W. Liu, X. Li, Metal-organic frameworks-derived Co₃O₄/Ti₃C₂T_x Mxene nanocomposites for high performance ethanol sensing, Sensor. Actuator. B Chem. 369 (2022), 132232.
- [60] W. Luo, Y. Sun, Y. Han, J. Ding, T. Li, C. Hou, Y. Ma, Flexible Ti₃C₂T_x MXene/polypyrrole composite films for high-performance all-solid asymmetric supercapacitors, Electrochim. Acta 441 (2023), 141818.
- [61] S. Yang, R. Yang, Z. Lin, X. Wang, S. Liu, W. Huang, Z. Chen, J. Wei, Z. Zeng, H. Chen, Ultrathin, flexible, and high-strength polypyrrole/Ti₃C₂T_x film for wideband gigahertz and terahertz electromagnetic interference shielding, J. Mater. Chem. A 10 (44) (2022) 23570–23579.
- [62] C. Zheng, Y. Yao, X. Rui, Y. Feng, D. Yang, H. Pan, Y. Yu, Functional MXene-based materials for next-generation rechargeable batteries, Adv. Mater. (2022), 2204988.
- [63] C. Li, J. Xu, Q. Xu, G. Xue, H. Yu, X. Wang, J. Lu, G. Cui, G. Gu, Synthesis of Ti₃C₂ MXene@PANI composites for excellent anticorrosion performance of waterborne epoxy coating, Prog. Org. Coating 165 (2022), 106673.
- [64] V. Krylova, N. Dukštienė, Synthesis and characterization of Ag₂S layers formed on polypropylene, J. Chem. 2013 (2013), 987879.
- [65] A. Gopanna, R.N. Mandapati, S.P. Thomas, K. Rajan, M. Chavali, Fourier transform infrared spectroscopy (FTIR), Raman spectroscopy and wide-angle X-ray scattering

(WAXS) of polypropylene (PP)/cyclic olefin copolymer (COC) blends for qualitative and quantitative analysis, Polym. Bull. 76 (8) (2019) 4259–4274.

Carbon 216 (2024) 118565

- [66] A. Adhikari, P. Tiwary, D. Rana, A. Halder, J. Nath, A. Basu, D. Ghoshal, P. Kar, A. K. Chakraborty, D. Chattopadhyay, Na-cholate micelle mediated synthesis of polypyrrole nanoribbons for ethanol sensing, J. Environ. Chem. Eng. 8 (5) (2020), 104249.
- [67] S. Cui, L. Yang, J. Wang, X. Wang, Fabrication of a sensitive gas sensor based on PPy/TiO₂ nanocomposites films by layer-by-layer self-assembly and its application in food storage, Sensor. Actuator. B Chem. 233 (2016) 337–346.
- [68] W.Y. Chen, S.-N. Lai, C.-C. Yen, X. Jiang, D. Peroulis, L.A. Stanciu, Surface functionalization of Ti₃C₂T_x MXene with highly reliable superhydrophobic protection for volatile organic compounds sensing, ACS Nano 14 (9) (2020) 11490–11501.
- [69] A. VahidMohammadi, J. Moncada, H. Chen, E. Kayali, J. Orangi, C.A. Carrero, M. Beidaghi, Thick and freestanding MXene/PANI pseudocapacitive electrodes with ultrahigh specific capacitance, J. Mater. Chem. A 6 (44) (2018) 22123–22133.
- [70] X. Chen, F. Su, Q. Zhou, J. Sun, High-performance all-solid-state flexible asymmetric supercapacitors composed of PPy@Ti₃C₂T_x/CC and Ti₃C₂T_x/CC electrodes, Surface. Interfac. 26 (2021), 101393.
- [71] X. Li, J. Xu, Y. Jiang, Z. He, B. Liu, H. Xie, H. Li, Z. Li, Y. Wang, H. Tai, Toward agricultural ammonia volatilization monitoring: a flexible polyaniline/Ti₃C₂T_x hybrid sensitive films based gas sensor, Sensor. Actuator. B Chem. 316 (2020), 128144
- [72] S.F. Hashemi Karouei, H. Milani Moghaddam, S. Saadat Niavol, Characterization and gas sensing properties of graphene/polyaniline nanocomposite with long-term stability under high humidity, J. Mater. Sci. 56 (6) (2021) 4239–4253.
- [73] Y. Fu, H. He, T. Zhao, Y. Dai, W. Han, J. Ma, L. Xing, Y. Zhang, X. Xue, A self-powered breath analyzer based on PANI/PVDF piezo-gas-sensing arrays for potential diagnostics application, Nano-Micro Lett. 10 (2018) 1–12.
- [74] S.H. Lee, W. Eom, H. Shin, R.B. Ambade, J.H. Bang, H.W. Kim, T.H. Han, Room-temperature, highly durable Ti(3)C(2)T(x) MXene/graphene hybrid fibers for NH (3) gas sensing, ACS Appl. Mater. Interfaces 12 (9) (2020) 10434–10442.
- [75] K. Namsheer, C.S. Rout, Conducting polymers: a comprehensive review on recent advances in synthesis, properties and applications, RSC Adv. 11 (10) (2021) 5659–5697.
- [76] J. Chung, S.H. Park, E.-H. Kim, S.I. Woo, Photoelectrochemical production of useful fuels from carbon dioxide on a polypyrrole-coated p-ZnTe photocathode under visible light irradiation, J. Mater. Chem. A 3 (3) (2015) 1089–1095.
- [77] G. Wu, H. Du, K. Pakravan, W. Kim, Y.L. Cha, S.-T. Chiang, M. Beidaghi, X. Zhang, S.H. Kim, X. Pan, Polyaniline/Ti₃C₂T_x functionalized mask sensors for monitoring of CO₂ and human respiration rate, Chem. Eng. J. (2023), 146228.
- [78] Y. Zhou, Y. Wang, Y. Wang, X. Li, Humidity-enabled ionic conductive trace carbon dioxide sensing of nitrogen-doped Ti₃C₂T_x MXene/polyethyleneimine composite films decorated with reduced graphene oxide nanosheets, Anal. Chem. 92 (24) (2020) 16033–16042.